Study on the Algorithm to Retrieve Precipitation with X-Band Synthetic Aperture Radar*

XIE Yanan[1†](谢亚楠), HUAN Jianping[1](还剑平), and TAO Yang[2](陶 阳)

1 *School of Communication and Information Engineering, Shanghai University, Shanghai* 200072, China

2 *University of Maryland, Maryland, MD* 21250, USA

(Received June 13, 2009; revised November 30, 2009)

ABSTRACT

In order to obtain the global precipitation distribution data, this paper investigates the precipitation distribution model, the normalized radar cross-section model, and the retrieval algorithm with X-band synthetic aperture radar (X-SAR). A new retrieval algorithm based on the surface-scattering reference attenuation is developed to retrieve the rain rate above the ground surface. This new algorithm needs no statistical work load and has more extensive applications. Calculations using the new algorithm for three cases verify that the rainfall is retrieved with high precision, which proves the capability of the algorithm.

Key words: microwave remote sensing, precipitation, retrieval algorithm, X-band synthetic aperture radar (X-SAR)

Citation: Xie Yanan, Huan Jianping, and Tao Yang, 2010: Study on the algorithm to retrieve precipitation with X-band synthetic aperture radar. *Acta Meteor. Sinica*, **24**(5), 614–621.

1. Introduction

Precipitation is a very important physical quantity in the research of the atmosphere, ocean, water, and environment. Global precipitation distribution and its vertical structure are the major weak points in the studies of current global climate and environmental changes. Only a few nations can acquire reliable data of global precipitation distribution. Precipitation plays a very important role in the overall atmospheric energy transmission, and it redistributes the global humidity and heat to a certain extent. Accurate measurement of precipitation is important to meteorological disaster forecasting, disaster prevention and mitigation, industrial production arrangements, agricultural planning, etc.

The Tropical Rainfall Measuring Mission (TRMM) is a joint project between the US National Aeronautics and Space Administration (NASA) and the Japan Aerospace Exploration Agency. It is designed to monitor and study tropical rainfall. The Global Precipitation Mission (GPM) of NASA is an outgrowth of TRMM that aims to improve precipitation measurements and to extend those measurements to higher latitudes. The GPM core satellite will carry Ku- and Ka-band radars, as well as an improved microwave radiometer.

Space-borne synthetic aperture radar (SAR) is a pulse Doppler radar used for two-dimensional imaging and generally not designed for atmospheric observations. SAR is considered as an "all weather" sensor. However, there is relevant theoretical and experimental evidence that X-band SAR (X-SAR hereafter) observations may be significantly affected by precipitation occurrences within the detection area. The high spatial-resolution observations of X-SAR serve as a new data source for obtaining the accurate global precipitation distribution.

Altas and Moore (1987) studied the radar equation and spatial resolution for precipitation measurement with SAR and showed that the precipitation distribution could be derived from the normalized radar cross-section (NRCS). Jameson et al. (1997), Moore et al. (1997), and Melsheimer et al. (1998) showed that X-SAR data can provide new insights into the structure of rain clouds and the mean rain

*Supported by the Science and Technology Commission of Shanghai Municipality under Grant No. 08590700500.

†Corresponding author: yxie@shu.edu.cn.

rate can be derived by using the data from SIR-C (Shuttle Imaging Radar-C)/X-SAR. Weinman and Marzano (2008) developed the X-SAR responses model and model-oriented statistical (MOS) algorithm to retrieve the shape, width, and other simple features of the vertical rainfall distribution according to the precipitation model developed by Yuter and Houze (1995).

The MOS algorithm is a statistical algorithm that retrieves the features of the precipitation distribution based on a large amount of statistics on SAR precipitation echoes. The empirical weighted coefficients of the MOS algorithm must be modified when the incident angle changes. This enhances the complexity and the statistical work load of the MOS algorithm.

A more analytical retrieval algorithm based on the surface-scattering reference attenuation is developed to retrieve rainfall above the ground surface in this paper. This algorithm can avoid the statistical work load and has a more extensive application.

2. The precipitation distribution model and the NRCS model

Marzano et al. (2006) developed a simple NRCS model using X-SAR data to obtain rainfall. Figure 1 shows a schematic view of a cloud scanning from the left by an X-SAR. The cross-track scan direction is x, the along-track scan direction is y, and the vertical direction is z; the incident angle of the slant SAR view is indicated by θ. The origin of the precipitation can be set at $x_{\rm L}=z_h/\tan\theta$. Microwave pulses emitted by the radar are approximated by plane wave front slices, and the SAR resolution in rain may be divided into three components:

$$V = r_{\rm R} \cdot r_{\rm c} \cdot r_{\rm a}, \tag{1}$$

where $r_{\rm a}$ is the along-track resolution, $r_{\rm c}$ the cross-track resolution, and $r_{\rm R}$ the slant-range resolution.

The total NRCS measured signal $\sigma_{\rm PSAR}$ consists of two components, backscattering from the surface $\sigma_{\rm srf}$ and volume backscattering by the precipitation $\sigma_{\rm vol}$, i. e.,

$$\sigma_{\rm PSAR} = \sigma_{\rm srf} + \sigma_{\rm vol}, \tag{2}$$

where (Marzano et al., 2006)

$$\sigma_{\rm srf} = \sigma^0 e^{-2\int_0^\infty k(x,z){\rm d}z/\cos\theta}, \tag{3}$$

$$\sigma_{\rm vol} = \int_0^\infty \eta(x,z) e^{-2\int_z^\infty k(x',z'){\rm d}z'/\cos\theta}{\rm d}z, \tag{4}$$

in which σ^0 is the surface radar cross-sectional coefficient, k is the extinction coefficient, and η is the radar volume reflectivity. The relations between k, η, and the rain rate $R(x,z)$ are

$$k(x,z) = a[R(x,z)]^b, \tag{5}$$

$$\eta(x,z) = \frac{\pi^5}{\lambda^4}|K|^2 Z_e, \tag{6}$$

$$Z_e = iR(x,z)^j, \tag{7}$$

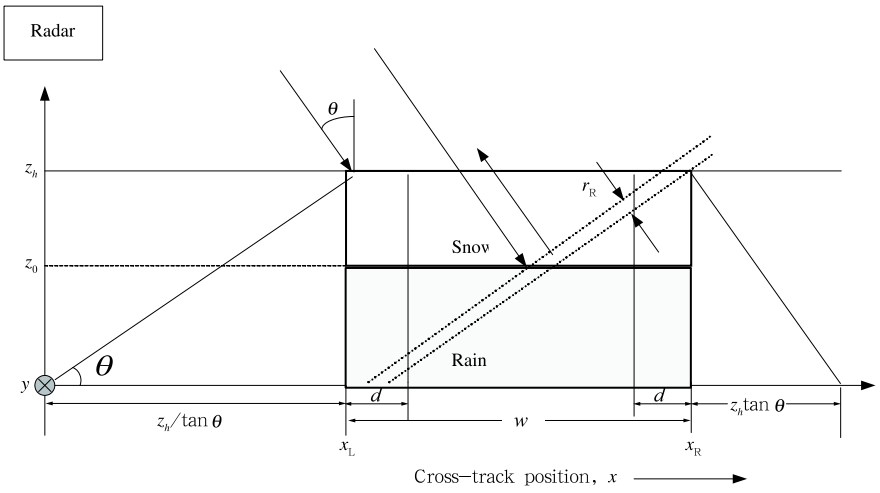

Fig. 1. Schematic view of the precipitation and the NRCS model.

where Z_e is the Rayleigh equivalent reflectivity factor; $|K|^2$ is a function of the refractive index, which is equal to about 0.93 for water and 0.19 for ice; λ is the wavelength, $\lambda = 3.1$ cm for X-band; a, b, i, and j are empirical coefficients depending on the wavelength and precipitation regime. Their typical values for continental convective rain clouds at X-band are as follows: $a = 2.6\times10^{-3}$, $b = 1.11$, $i = 300$, $j = 1.35$ for rain and $a = 5.6\times10^{-5}$, $b = 1.6, i = 182, j = 1.6$ for snow with predominant scattering behavior, according to Ulaby et al. (1981).

A simple precipitation distribution model that considers various vertical and horizontal distributions is expressed in the form (Weinman and Marzano, 2008):

$$R(x,z) = H(x)\cdot V(z), \tag{8}$$

where $H(x)$ is the horizontal precipitation distribution, determined by the width w and the shape parameter d. The common distributions are rectangular distribution ($d = 0$), triangular distribution ($d = w/2$), and trapezoidal distribution ($0 < d < w/2$). $V(z)$ is the vertical distribution, and an analytic approximation of $V(z)$ (Marzano et al., 2008) is

$$V(z) = \begin{cases} V(0)\cdot V_{\rm r}(z) = V(0)[0.85 & \\ +0.15(\dfrac{z_0 - z}{z_0})^{0.62}], & 0 \leqslant z \leqslant z_0, \quad (9) \\ V(0)\cdot V_{\rm s}(z) = 0.85V(0) & \\ \cdot(\dfrac{z_h - z}{z_h - z_0})^p, & z_0 \leqslant z \leqslant z_h, \quad (10) \end{cases}$$

where z_0 is the height of the freezing level and z_h is the height of the top of the frozen precipitation; $V(0)$ is the rain rate at ground; the parameter p defines the diminished rate of the frozen hydrometeor, and its typical value is 0.5.

Assume $w = 10$ km, $\lambda = 3.1$ cm, $z_0 = 4.5$ km, $z_h = 13$ km, $V(0) = 100$ mm h^{-1}, $\theta = 30°$, $\sigma^0 = -7$ dB, and $p = 0.5$. Figure 2 shows the NRCS scan of the rectangular ($d = 0$), trapezoidal ($d = 3$ km), and triangular ($d = 5$ km) precipitation distributions as a function of cross-track scanning distance.

As the X-SAR scans from left to right, the NRCS first increases to above the background value due to the scattering by the frozen hydrometeors in the upper part of the cloud. As the X-SAR continues to scan further to the right, the signal from the underlying surface is reduced by radiation attenuation due to the rain. The NRCS increases again as the scanned footprint moves to the right beyond the precipitating cloud, and less rain is intercepted.

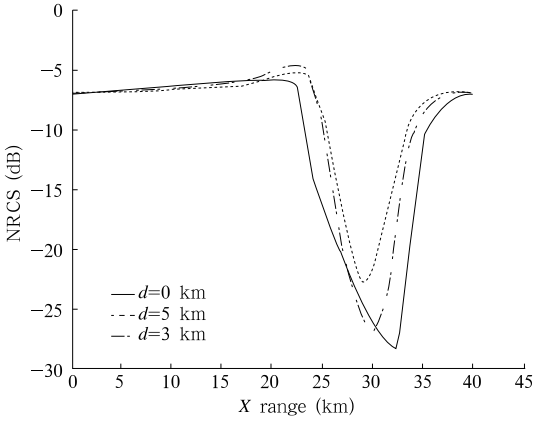

Fig. 2. Comparison of the NRCS scans of three different distributions.

3. MOS precipitation retrieval algorithm

The MOS precipitation retrieval algorithm was developed by Weinman and Marzano (2008). The purpose of MOS is to exploit the basic features of the measured NRCS profile built upon the forward precipitation model. Assume that the values of z_h, z_0, and θ are known, the algorithm can retrieve $V(0), p, w$, and d of the rainfall distribution model.

The algorithm first finds a crossing node x_0, where the NRCS makes a transition from enhancement due to scattering to reduction due to attenuation. The identification of the $H(x)$ shape parameter d is carried out statistically, based on the maximum-likelihood metric concept. The MOS algorithm then retrieves the width of the precipitation, which uses the locations of x_0 and the minimum NRCS location $x_{\rm min}$. Thus, the horizontal function $H(x)$ can be identified.

The next procedure is to retrieve the parameter $V(0)$ and p of the vertical profile $V(z)$ given in Eqs. (9) and (10), then to reconstruct the rainfall distribution $R(x,z)$. The overall MOS method is schematically shown in Fig. 3 (Marzano et al., 2008).

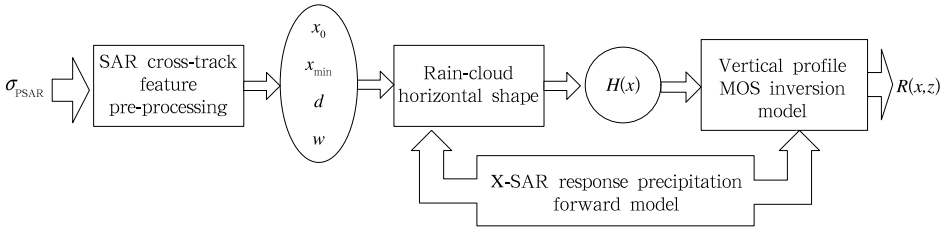

Fig. 3. Schematic view of the MOS algorithm (Marzano et al., 2008).

The retrieved surface rainfall by the MOS algorithm for $\theta = 30°$ is:

$$V(0) = 1.13 \int_{x_0}^{x_{\max}} [\mathrm{d}B\sigma^0 - \mathrm{d}B\sigma_{\mathrm{PSAR}}(x)]\mathrm{d}x$$
$$-21.62 \int_0^{x_0} [\sigma_{\mathrm{PSAR}}(x) - \sigma^0]\mathrm{d}x - 2.58w + 23.3. \quad (11)$$

The first integral in the above equation is proportional to the difference of the algorithm of the background and that of the NRCS over the region $x_0 \leqslant x \leqslant x_{\max}$ where the σ_{PSAR} is strongly attenuated by rain. The second integral is a function of the difference between the background and the precipitation cross-sections where the scattering signature of the snowfall is dominant. The last term accounts for the dependence on the width of $H(x)$.

The weighted coefficients of Eq. (11) are only appropriate for $\theta = 30°$ when using the MOS algorithm. They must be modified as the radar incident angle changes. Thus, too much statistical work has to be done to obtain all the weighted coefficients for different incident angles and the accuracy of the algorithm is reduced. Moreover, the dependence of the algorithm on the retrieved width of the precipitation also reduces the accuracy.

4. Surface-scattering reference attenuation retrieval algorithm

To reduce the statistical work and to find a more analytical rainfall retrieval algorithm, we propose a surface-scattering reference attenuation (SRA) algorithm to retrieve the rainfall above the ground surface.

The solution of the X-SAR integral Eqs. (3) and (4) requires the extraction of path-integrated quantities. It should be noted that the surface reflection term σ_{srf} mainly depends on the extinction coefficient of the rain, which is more closely related to the rainfall than the effective radar reflectivity factor. The latter is more sensitive to the drop size distribution than the extinction coefficient. The difference between σ_{srf} within rain and σ_{srf} outside the rain area can be used to estimate the rainfall. As both σ_{srf} and σ_{vol} contribute to σ_{PSAR}, separating σ_{srf} from σ_{PSAR} is a basic step of the SRA algorithm.

As the beam scans over the region of precipitation, the backscattered power from the surface is affected by both σ^0 and the attenuation factor. The parameter σ^0 at different geographic locations can be obtained from a previous measurement made in the absence of precipitation. In the SRA algorithm, the actual σ^0 can be approximated by an average value of σ^0 measured in the rain-free area adjacent to the target. A typical value of σ^0 for vertically polarized X-band radiation at the 30° incident angle over rough land surface is –7 dB, and σ^0 at other incident angles can be found in Oh et al. (1992).

When X-SAR scans on the right edge of the precipitation cell as shown in Fig. 1, σ_{vol} is very low due to no volume scattering. There are two cases for the attenuation path of the surface scattering that should be considered: 1) $z_h \cdot \tan\theta \leqslant w$, the rain cell is long enough for a complete attenuation path from top to ground within the rain cell; 2) $z_h \cdot \tan\theta > w$, the attenuation path is from the top of the rain but it cannot reach the ground within the rain cell, therefore there is less attenuation.

To make a simple model, we only consider case 1. At the right edge of the precipitation cell, the minimum NRCS can be found as σ_{vol} is nearly zero and the attenuation path of σ_{srf} is the largest.

Figure 4a shows details of σ_{srf} and σ_{vol} when X-SAR scans a rectangular precipitation distribution cell. Figure 4b shows the percentage of σ_{srf} in σ_{PSAR},

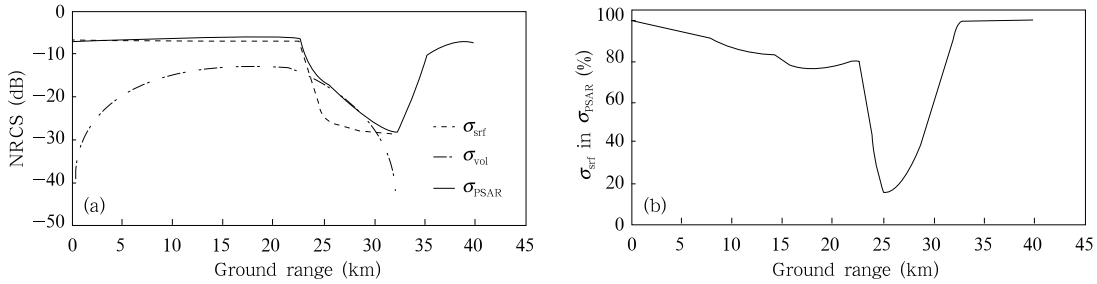

Fig. 4. (a) NRCS scans for $\sigma_{\rm srf}$, $\sigma_{\rm vol}$, and $\sigma_{\rm PSAR}$; (b) percentages of $\sigma_{\rm srf}$ in $\sigma_{\rm PSAR}$.

which indicates the dominant portion of $\sigma_{\rm srf}$ at the minimum NRCS, so $\sigma_{\rm vol}$ can be neglected in this area. According to Eqs. (2) and (3), we obtain

$$\sigma_{\min} \approx \sigma_{\rm srf} = \sigma^0 e^{-2\int_0^\infty k(x,z){\rm d}z/\cos\theta}, \tag{12}$$

where $\sigma_{\min}$ is the minimum of $\sigma_{\rm PSAR}$. It is followed by

$$\int_0^\infty k(x,z){\rm d}z \approx -\frac{1}{2}\ln(\sigma_{\min}/\sigma^0)\cdot\cos\theta. \tag{13}$$

Substituting Eqs. (5) and (8) into Eq. (13), we obtain

$$\int_0^\infty a[H(x)V(z)]^b{\rm d}z = -\frac{1}{2}\ln(\sigma_{\min}/\sigma^0)\cdot\cos\theta. \tag{14}$$

According to Eqs. (9) and (10), Eq. (14) can be written as

$$\begin{aligned}&\int_0^{z_0} a_1[H(x)V(0)V_r(z)]^{b_1}{\rm d}z\\ &+\int_{z_0}^{z_h} a_2[H(x)V(0)V_s(z)]^{b_2}{\rm d}z\\ &=-\frac{1}{2}\ln(\sigma_{\min}/\sigma^0)\cdot\cos\theta,\end{aligned} \tag{15}$$

where a_1 and b_1 are known for rain; a_2 and b_2 are known for snow.

Extracting the parameter V(0) from the integrals, we finally obtain

$$\begin{aligned}&a_1V(0)^{b_1}\int_0^{z_0}[H(x)V_r(z)]^{b_1}{\rm d}z\\ &+a_2V(0)^{b_2}\int_{z_0}^{z_h}[H(x)V_s(z)]^{b_2}{\rm d}z\\ &=-\frac{1}{2}\ln(\sigma_{\min}/\sigma^0)\cdot\cos\theta,\end{aligned} \tag{16}$$

where $H(x) = H(x_{\min} - z\cdot\tan\theta)$, and $x_{\min}$ is the position of $\sigma_{\min}$. Equation (16) can be solved by dichotomy to obtain the ground surface rain rate $V(0)$.

The first procedure of the SRA algorithm is to retrieve the horizontal precipitation $H(x)$, which is the same as the MOS retrieval algorithm. After $H(x)$ is classified, the SRA algorithm retrieves the vertical precipitation distribution.

To retrieve $V(0)$, some simplifying assumptions are needed as in all rainfall retrieval algorithms with a single-frequency radar. Under these assumptions, the surface scattering σ^0 is constant, which is the same as that in the TRMM-PR surface-reference technique (Iguchi et al., 2000); the attenuation coefficient and rain rate law shown in Eq. (5) are assumed known; a sharp transition exists between rain and snow at the freezing height.

The SRA retrieval algorithm assumes that the parameters z_h, z_0, θ, and p are known. The paramete z_h can be determined by the first received radar echo and the height of the satellite. The freezing level height z_0 could be determined from surface temperature by assuming that the lapse rate is 5.8°C km^{-1} (Wu and Weinman, 1984), or from temperature profiles obtained by radiosonde. The parameter θ is the SAR output parameter. The parameter p usually takes the typical value of 0.5.

The SRA algorithm can work at any incident angle of SAR and no modification of the weighted coefficients is needed. This is distinct from the MOS, and therefore the SRA method can significantly reduce the statistical work and has more extensive applications.

5. Simulated retrieval results

We present a comparison between three different rain distributions and the retrieval results by the SRA algorithm. The SAR scan data can be simulated by

the NRCS model described in Eqs. (2)–(7).

Example 1: the horizontal distribution is rectangular, $V(0) = 100$ mm h^{-1}, $w = 10$ km, $d = 0$, $z_h = 13$ km, $z_0 = 4.5$ km, $\theta = 30°$, $\sigma^0 = -7$ dB, and $p = 0.5$. The retrieved ground surface rain rate is 113 mm h^{-1}, and the error is 13% (Fig. 5).

Example 2: the horizontal distribution is triangular, $V(0) = 150$ mm h^{-1}, $w = 10$ km, $d = 5$ km, $z_h = 10$ km, $z_0 = 4$ km, $\theta = 20°$, $\sigma^0 = -6$ dB, and p=0.5. The retrieved ground surface rain rate is 152.0 mm h^{-1}, and the error is 1.3% (Fig. 6).

Example 3: the horizontal distribution is trapezoidal, $V(0) = 50$ mm h^{-1}, $w = 10$ km, $d = 3$ km, $z_h = 8$ km, $z_0 = 3.5$ km, $\theta = 35°$, $\sigma^0 = -8$ dB, and $p = 0.5$. The retrieved ground surface rain rate is 53.6 mm h^{-1}, and the error is 7.2% (Fig. 7).

From the retrieval results of the above examples, we can see that the SRA algorithm can be applied to any incident angle and different horizontal distributions. A fairly good consistency is displayed by comparing the simulated and retrieved rain rates. The error of the retrieval results compared with the real rainfall distribution is within 15%, which is mainly caused by neglecting the volume scattering.

The retrieved surface rainfall by the MOS algorithm at $\theta = 30°$ is shown in Eq. (11). We present

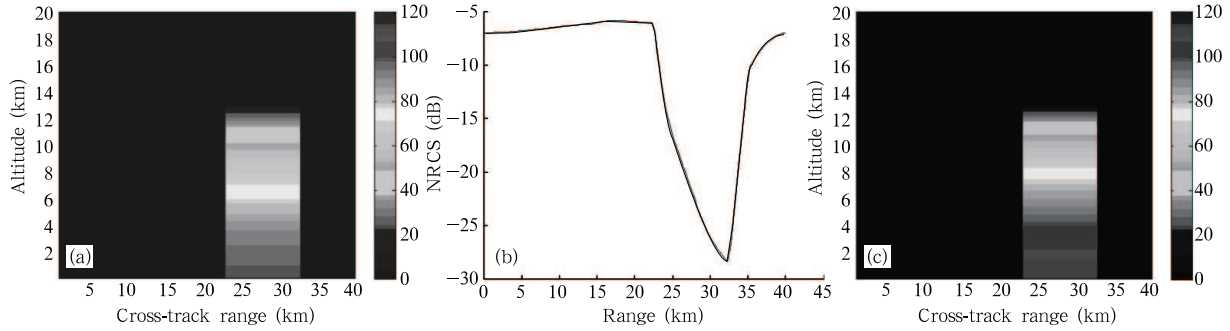

Fig. 5. (a) Real distribution, (b) NRCS scans, and (c) the SRA retrieval for Example 1.

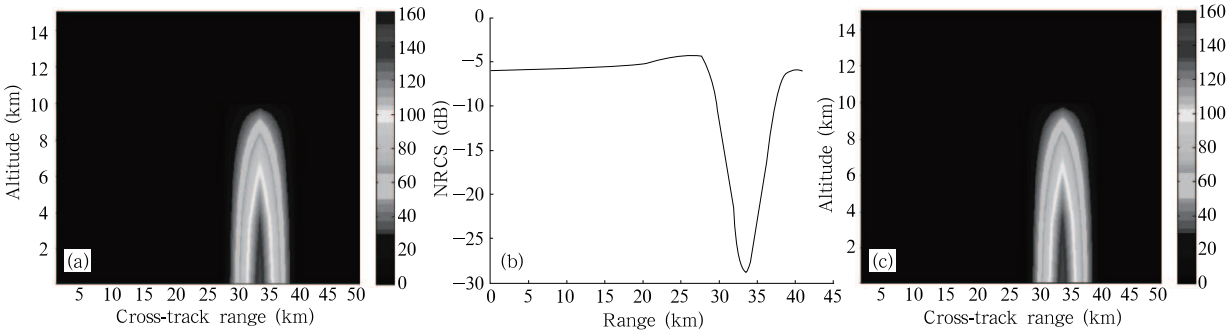

Fig. 6. As in Fig. 5, but for Example 2.

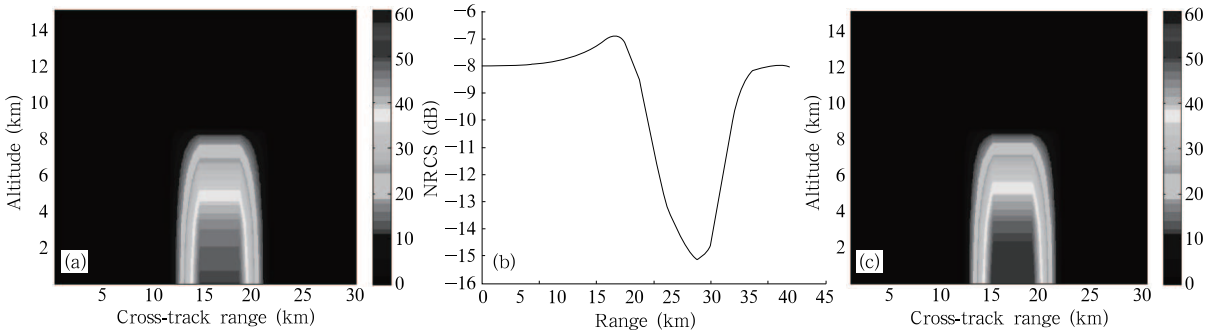

Fig. 7. As in Fig. 5, but for Example 3.

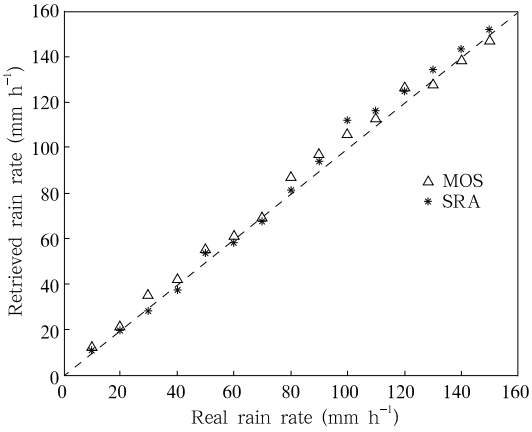

Fig. 8. Comparison of the SRA and the MOS algorithms.

a comparison of the retrieved results between the MOS and SRA algorithms in Fig. 8. The related parameters are the same as those in the above three examples except that $V(0)$ is from 10 to 150 mm h^{-1}.

The relative error of the surface rainfall $V(0)$ is given by

$$\mathrm{RMS}_n = \sqrt{\frac{1}{n}\sum_{i=1}^{n}\left[\frac{\hat{V}(0)-V(0)}{V(0)}\right]^2}, \qquad (17)$$

where $\hat{V}(0)$ is the retrieved ground surface rainfall. The RMS_n is 8.35% for the MOS algorithm and 5.87% for the SRA algorithm. The SRA algorithm gets a better consistency between the simulated and retrieved fields than the MOS algorithm. This is mainly because the SRA assumes that p is known, which enhances the accuracy.

The precision of the SRA algorithm is associated with the value of p. The latter has a limited influence on the retrieval accuracy because σ^0 attenuated by the snow layer is much lower than that by the rain layer, according to the attenuation coefficient and rain rate law in Eq. (5) and the empirical coefficients a and b for rain and snow.

6. Conclusions

This paper employs a new rainfall retrieval algorithm based on the measured NRCS data to reconstruct the rainfall distribution. An NRCS model is set up to simulate the SAR response to rainfall. A simple precipitation distribution model derived from various vertical and horizontal distributions permits us to account for some features of the NRCS response. Differences in the appearance of these NRCS scans illustrate that the rainfall distribution could be derived from NRCS scans.

The MOS algorithm based on the statistical method is developed to infer the rainfall distribution. Parameters describing the rainfall distribution are retrieved from the features of the NRCS scans. However, the MOS algorithm needs considerable statistical work to obtain different weighted coefficients at different incident angles as shown in Eq. (11).

We have proposed a more analytical rainfall retrieval algorithm–the SRA algorithm, to reduce the tedious statistical work and to retrieve the rainfall above the ground surface. The surface backscattering occupies the dominant part at the measured minimum of NRCS. The SRA algorithm neglects the influence of volume scattering at that point and retrieves the rain rate. The SRA method can be used at any incident angle, which enhances its applications. Different precipitation distributions are retrieved from the simulated NRCS data by the SRA algorithm. The MOS and SRA schemes produce consistent results in comparison. As in all rainfall retrieval approaches based on the radar data, some simplifying assumptions are needed. In the future, we will investigate if the SRA algorithm can be further improved with fewer assumption conditions.

REFERENCES

Atlas, D., and R. K. Moore, 1987: The measurement of precipitation with synthetic aperture radar. *J. Atmos. Ocean. Tech.*, **4**(3), 368–376.

Iguchi, T., et al., 2000: Rain profiling algorithm for the TRMM precipitation radar. *J. Appl. Meteor.*, **39**, 2038–2052.

Jameson, R., et al., 1997: SIR-C/X-SAR observations of rain storms. *Remote Sens. Environ.*, **59**(2), 267–279.

Marzano, F. S., et al., 2006: Rain retrieval over land from X-band spaceborne synthetic aperture radar. The Fourth European Conference on Radar Meteorology and Hydrology (ERAD 2006), Barcelona, 18–21.

——, et al., 2008: Inversion of spaceborne X-band synthetic aperture radar measurements for precipita-

tion remote sensing over land. *IEEE Transactions on Geoscience and Remote Sensing*, **46**(11), 3472–3487.

Melsheimer, C., et al., 1998: Investigation of multifrequency/multipolarization radar signatures of rain cells derived from SIR-C/X-SAR data. *J. Geophy. Res.*, **103**, 18867–18884.

Moore, R. K., et al., 1997: Rain measurement with SIR-C/X-SAR. *Remote Sens. Environ.*, **59**(2), 280–293.

Oh, Y., et al., 1992: An empirical model and an inversion technique for radar scattering from bare soil surfaces. *IEEE Trans. Geosci. Remote Sens.*, **30**, 370–381.

Ulaby, F. T., et al., 1981: *Microwave Remote Sensing Fundamentals and Radiometry. Vol. I. Microwave Remote Sensing, Active and Passive.* Artech House, 321–327.

Weinman, J. A., and F. S. Marzano, 2008: An exploratory study to derive precipitation over land from X-band synthetic aperture radar measurements. *J. Appl. Meteor. Climatol.*, **47**(2), 562–575.

Wu, R., and J. A. Weinman, 1984: Microwave radiances from precipitating clouds containing aspherical ice, combined phase, and liquid hydrometeors. *J. Geophys. Res.*, **89**(5), 7170–7178.

Yuter, S. E., and R. A. Houze, 1995: Three-dimensional kinematical and microphysical evolution of Florida cumulonimbus. Part II: Frequency distributions of vertical velocity, reflectivity, and differential reflectivity. *Mon. Wea. Rev.*, **123**(7), 1941–1963.